

---

# Conditional Diffusion Models for Uncertainty Estimation in Super Resolution Microscopy

---

Anonymous Author(s)

Affiliation

Address

email

## Abstract

1 The field of deep generative modeling for image translation has experienced a  
2 boom in research in the past few years, with various tools developed to estimate  
3 different types of uncertainty. Yet, many powerful models in image translation  
4 are selected and trained under a simple reconstruction loss and therefore are un-  
5 able report uncertainty in their outputs. Uncertainty quantification is a necessary  
6 modeling component in many high-risk applications and in the sciences. In order  
7 to quantify uncertainty in otherwise deterministic models, we propose a hybrid  
8 generative modeling framework based denoising diffusion probabilistic models  
9 (DDPMs). Specifically, our model learns a distribution on the true image latent  
10 in the input conditioned on the network output, in order to represent the posterior  
11 on reconstructions. Then, we apply this framework to the task of single molecule  
12 localization in fluorescence microscopy, and demonstrate that blending the Deep-  
13 STORM architecture with a DDPM permits uncertainty quantification of kernel  
14 density estimates (KDEs) regressed by DeepSTORM. Our results suggest the pro-  
15 posed solution is an interesting addition to the modeling toolkit for fluorescence  
16 microscopists and the field of deep image translation in general.

## 17 1 Introduction

18 Deep learning has attracted tremendous attention from researchers in fields such as physics, biology,  
19 and manufacturing, to name a few (Baldi et al., 2014; Anjos et al., 2015; Bergmann et al., 2014).  
20 Tools such as neural networks (NNs), dropout, convolutional neural networks (convnets), and others  
21 are used extensively. In particular, the application of deep image translation in single-molecule  
22 localization microscopy (SMLM) has received considerable interest (Ouyang 2018; Nehme 2020;  
23 Speiser 2021). SMLM techniques are a mainstay of fluorescence microscopy and can be used to  
24 produce a pointillist representation of living cells at diffraction-unlimited precision. As this technology  
25 enables increasingly precise measurements of the cellular environment, there is an increasing need  
26 for machine learning methods to report uncertainty for quality control.

27 In previous applications of deep models to localization microscopy, super-resolution images can be  
28 recovered from a sparse set of localizations with conditional generative adversarial networks (Ouyang  
29 2018) or kernel density estimation can be performed using convolutional networks (Nehme 2020;  
30 Speiser 2021). Here, we focus on the latter class of models which perform single molecule localization  
31 using neural networks. In this approach, one estimates molecular coordinates by predicting kernel  
32 density estimates (KDEs)  $y$ , which are latent in the raw data  $x$ , using a convolutional neural network.  
33 Importantly, inferences in SMLM are often necessarily made on a single measurement, thus common  
34 measures of model performance are based on localization errors computed over ensembles of  
35 simulated images. However, this choice precludes computation of aleatoric uncertainty at test time  
36 under a fixed model, and may result in the application of models to out of distribution datasets.



Figure 1: Generative model of single molecule localization microscopy images

Bayesian probability theory offers us mathematically grounded tools to reason about model uncertainty, but these usually come with a prohibitive computational cost. Recent approaches to avoiding this intractability have been deterministic uncertainty quantification (Amersfoort 2020), ensembling (Lakshminarayanan et al., 2017) or Monte Carlo sampling (Gal and Ghahramani, 2016). Here, we report a method which models estimates uncertainty in KDE predictions by learning a distribution on the true image latent in the input conditioned on the network output, in order to represent the posterior on reconstructions. Our approach preserves image structure and produces pixel-wise uncertainties, which can be used for out of distribution sample detection or filtering. Our approach could be readily integrated with existing localization performance measures to address both model accuracy on training data and precision on datasets produced by experiments.

## 2 Background

### 2.1 Image Likelihood and Localization Error

The central objective of single molecule localization microscopy is to infer a set of molecular coordinates from measured low resolution images  $\mathbf{x}$ . The likelihood on measured low-resolution images  $p(\mathbf{x}|\theta)$  is taken to be a convolution of Gaussian and Poisson PDFs

$$p(\mathbf{x}_k|\theta) = A \sum_{q=0}^{\infty} \frac{1}{q!} e^{-\omega_k} \omega_k^q \frac{1}{\sqrt{2\pi}\sigma_k} e^{-\frac{(\mathbf{x}_k - g_k q - o_k)^2}{2\sigma_k^2}} \quad (1)$$

where  $p(\zeta_k) = \mathcal{N}(o_k, \sigma_k^2)$  and  $p(s_k) = \text{Poisson}(\omega_k)$ ,  $A$  is some normalization constant. In practice, (4) is difficult to work with, so we look for an approximation. We will use a Poisson-Normal approximation for simplification.

$$\mathbf{x}'_k \sim \text{Poisson}(\omega'_k) \quad (2)$$

where  $\omega'_k = \omega_k + \sigma_k^2$ . This result can be seen from the fact the the convolution of two Poisson distributions is also Poisson.

We use the Fisher information as an information theoretic criteria to assess the quality of the proposed algorithms, with respect to the root mean squared error (RMSE) of our predictions of  $\theta$ . The generative model  $\ell(\mathbf{x}|\theta)$  is also convenient for computing the Fisher information matrix (Smith 2010) and thus the Cramer-Rao lower bound, which bounds the variance of a statistical estimator of  $\theta$ , from below i.e.,  $\text{var}(\hat{\theta}) \geq I^{-1}(\theta)$ . It is shown in the appendix, that the Fisher information is straightforward to compute under the Poisson likelihood (7)

$$\mathcal{I}_{ij}(\theta) = \mathbb{E}_{\theta} \left( \frac{\partial \ell}{\partial \theta_i} \frac{\partial \ell}{\partial \theta_j} \right) = \sum_k \frac{1}{\omega'_k} \frac{\partial \omega'_k}{\partial \theta_i} \frac{\partial \omega'_k}{\partial \theta_j} \quad (3)$$

### 2.2 Kernel density estimation with deep networks

Direct optimization of the log-likelihood in (7) from observations  $\mathbf{x}$  alone is challenging when fluorescent emitters are dense within the field of view and fluorescent signals significantly overlap. Convolutional neural networks (CNN) have recently been used in fluorescence microscopy to extract

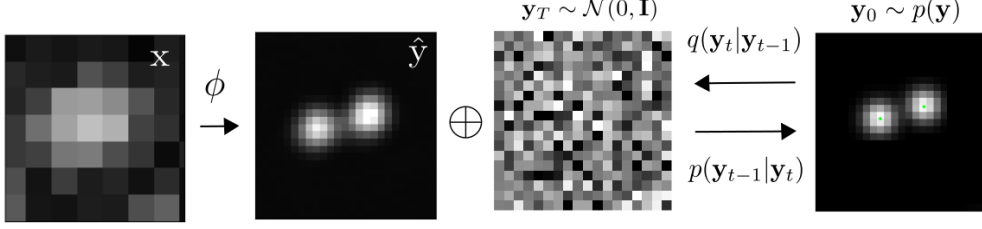


Figure 2: Conditional diffusion model for sampling kernel density estimates

parameters describing fluorescent emitters such as color, emitter orientation, z coordinate, background signal. For localization tasks, CNNs typically employ upsampling layers to reconstruct Bernoulli probabilities of emitter occupancy or kernel density estimates with higher resolution than experimental measurements. Kernel density estimates are the most common data structure used in SMLM, and can be easily generated from molecular coordinates using the optical impulse response (2). While ground-truth data from experiments to train the neural network are typically not available, synthetic training data can also be generated by (2) and simulation from the Poisson likelihood (7).

The DeepSTORM CNN, initially proposed in [1] for 3D localization, can be viewed as a deep kernel density estimator, reconstructing kernel density estimates  $\mathbf{y}$  from low-resolution inputs  $\mathbf{x}$ . We utilize a simplified form of the original architecture for 2D localization, which we denote  $\phi$  hereafter, which consists of three main modules: a multi-scale context aggregation module, an upsampling module, and a prediction module. For context aggregation, the architecture utilizes dilated convolutions to increase the receptive field of each layer. The upsampling module is then composed of two consecutive 2x resize-convolutions, computed by nearest-neighbor interpolation, to increase the lateral resolution by a factor of 4. For a common sCMOS camera, each pixel has a lateral size of approximately 108 nanometers, giving approximately 27 nanometer pixels in the KDE. The terminal prediction module contains three additional convolutional blocks for refinement of the upsampled image, followed by an element-wise HardTanh.

### 3 Denoising Diffusion Probabilistic Model for SMLM

We consider datasets  $(\mathbf{x}_i, \mathbf{y}_i, \hat{\mathbf{y}}_i)_{i=1}^N$  of observed images  $\mathbf{x}_i$  true kernel density estimate (KDE) images  $\mathbf{y}_i$ , and KDE estimates  $\hat{\mathbf{y}}_i = \phi(\mathbf{x}_i)$ . Observations  $\mathbf{x}_i$  are generated under the image degradation model. We aim to develop a framework for sampling from  $p(\hat{\mathbf{y}}|\mathbf{x}, \mathbf{y})$ .

### 4 Conditional Denoising Diffusion Model

Point estimates  $\hat{\mathbf{y}}_i$  produced by the DeepSTORM architecture lack uncertainty quantification. To address this, we propose a DDPM to model the conditional distribution  $p(\hat{\mathbf{y}}|\mathbf{x}, \mathbf{y})$ . Consider the factorization  $p(\hat{\mathbf{y}}|\mathbf{x}, \mathbf{y})p(\mathbf{x}|\mathbf{y})p(\mathbf{y}) = p(\mathbf{x}|\mathbf{y}, \hat{\mathbf{y}})p(\mathbf{y}|\hat{\mathbf{y}})p(\hat{\mathbf{y}})$ . Given that  $\mathbf{x}$  is conditionally independent of  $\hat{\mathbf{y}}$ , we find

$$p_{\Psi}(\hat{\mathbf{y}}|\mathbf{x}, \mathbf{y}) = p(\mathbf{y}|\hat{\mathbf{y}})$$

Evidently, the DDPM  $\Psi$  can be trained on pairs  $(\mathbf{y}_i, \hat{\mathbf{y}}_i)_{i=1}^N$ . The conditional DDPM generates a target KDE  $\mathbf{y}_0$  in  $T$  refinement steps. Starting with a pure noise image  $\mathbf{y}_T \sim \mathcal{N}(0, \mathbf{I})$ , the model iteratively refines the KDE through successive iterations according to learned conditional transition distributions  $p(\mathbf{y}_{t-1}|\mathbf{y}_t, \hat{\mathbf{y}})$  such that  $\mathbf{y}_0 \sim p(\mathbf{y}|\hat{\mathbf{y}})$ .

#### 4.1 Gaussian Diffusion

Diffusion models (Sohl-Dickstein 2015; Ho 2020) are a class of generative models inspired by nonequilibrium statistical physics, which slowly destroy structure in a data distribution  $p(\mathbf{y}_0|\mathbf{x})$  via a fixed Markov chain referred to as the *forward process*. In the present context, the forward process gradually adds Gaussian noise to the KDE  $\mathbf{y}$  according to a variance schedule  $\beta_{0:T}$ .

$$q(\mathbf{y}_t|\mathbf{y}_0) = \prod_{t=1}^T q(\mathbf{y}_t|\mathbf{y}_{t-1}) \quad q(\mathbf{y}_t|\mathbf{y}_{t-1}) = \mathcal{N}\left(\sqrt{1-\beta_t}\mathbf{y}_{t-1}, \beta_t \mathbf{I}\right) \quad (4)$$

103 An important property of the forward process is that it admits sampling  $\mathbf{y}_t$  at an arbitrary timestep  $t$   
 104 in closed form (Ho 2020). Using the notation  $\alpha_t := 1 - \beta_t$  and  $\gamma_t := \prod_{s=1}^t \alpha_s$ , we have

$$q(\mathbf{y}_t|\mathbf{y}_0) = \mathcal{N}(\sqrt{\gamma_t}\mathbf{y}_0, (1 - \gamma_t)\mathbf{I}) \quad (5)$$

105 The usual procedure is then to learn a parametric representation of the *reverse process*, and therefore  
 106 generate samples from  $p(\mathbf{y}_0)$ , starting from noise. Formally,  $p_\theta(\mathbf{y}_0|\hat{\mathbf{y}}) = \int p_\theta(\mathbf{y}_{0:T}|\hat{\mathbf{y}})d\hat{\mathbf{y}}_{1:T}$  where  
 107  $\mathbf{y}_t$  is a latent representation with the same dimensionality of the data.  $p_\theta(\mathbf{y}_{0:T}|\hat{\mathbf{y}})$  is a Markov process,  
 108 starting from a noise sample  $p_\theta(\mathbf{y}_T) = \mathcal{N}(0, \mathbf{I})$ .

$$p_\theta(\mathbf{y}_{0:T}) = p_\theta(\mathbf{y}_T) \prod_{t=1}^T p_\theta(\mathbf{y}_{t-1}|\mathbf{y}_t) \quad p_\theta(\mathbf{y}_{t-1}|\mathbf{y}_t) = \mathcal{N}(\mu_\theta(\mathbf{y}_t), \beta_t \mathbf{I}) \quad (6)$$

109 where we reuse the variance schedule of the forward process (Ho 2020). We seek to learn a denoising  
 110 model  $\mu_\theta$  which computes the mean of the Gaussian transition density at each time step  $t$ . For all  
 111  $t > 0$ , the mean of the transition density is computed as

$$\mu_\theta(\mathbf{y}_t, \hat{\mathbf{y}}, \gamma_t) = \frac{1}{\sqrt{\alpha_t}} \left( \mathbf{y}_t - \frac{(1 - \alpha_t)}{\sqrt{1 - \gamma_t}} f_\theta(\mathbf{y}, \hat{\mathbf{y}}, \gamma_t) \right) \quad (7)$$

112 where  $f_\theta$  is a neural network. Only at  $t = 0$  is this mean directly a function of  $\mathbf{x}$ .

## 113 4.2 Optimization of the Denoising Model

114 To reverse the diffusion process, we optimize a neural denoising model  $f_\theta$  that takes as input  $\hat{\mathbf{y}}$  and a  
 115 noisy target image  $\mathbf{y}_t \sim q(\mathbf{y}_t|\mathbf{y}_0)$ . That is, this noisy target image  $\mathbf{y}_t$  is drawn from the marginal  
 116 distribution of noisy images at a time step  $t$  of the forward diffusion process.

$$\mathbf{y}_t = \sqrt{\gamma_t}\mathbf{y}_0 + \sqrt{1 - \gamma_t}\epsilon, \quad \epsilon \sim \mathcal{N}(0, \mathbf{I}) \quad (8)$$

117 In addition to a source image  $\mathbf{y}_0$  and a noisy target image  $\mathbf{y}_t$ , the denoising model  $f_\theta$  takes as input  
 118 the sufficient statistics for the variance of the noise  $\gamma$ , and is trained to predict the noise vector  $\epsilon$ .  
 119 We make the denoising model aware of the level of noise through conditioning on a scalar  $\gamma$ . The  
 120 proposed objective function for training  $f_\theta$  is

$$\mathbb{E}_{(\hat{\mathbf{y}}, \mathbf{y}_0)} \mathbb{E}_{(\epsilon, \gamma)} \left[ f_\theta \left( x, \sqrt{\gamma}\mathbf{y}_0 + \sqrt{1 - \gamma}\epsilon \mid \mathbf{y}_t, \gamma \right) - \epsilon \right], \quad (9)$$

121 where  $(\hat{\mathbf{y}}, \mathbf{y}_0)$  is sampled from the training dataset and  $\gamma \sim p(\gamma)$ . The distribution of  $\gamma$  has a big  
 122 impact on the quality of the model and the generated outputs. For our training noise schedule, we  
 123 use a piecewise distribution for  $\gamma$ ,  $p(\gamma) = \frac{1}{T} \sum_{t=1}^T U(\gamma_{t-1}, \gamma_t)$  (Nanxin 2021). Specifically, during  
 124 training, we first uniformly sample a time step  $t \sim \{0, \dots, T\}$  followed by sampling  $\gamma \sim U(\gamma_{t-1}, \gamma_t)$ .  
 125 We set  $T = 100$  in all our experiments.

## 126 4.3 Optimization of the DeepSTORM architecture

127 A first pass at localization treats localization as a binary classification problem, such that 0 denotes  
 128 a vacant pixel and 1 denotes an occupied pixel containing an emitter. Direct learning of pixel-wise  
 129 classification with cross-entropy loss leads to an imbalance of occupied and unoccupied pixels in  
 130 dense localization problems (Nehme 2020). CE loss is usually either weighted [51], replaced with a  
 131 Focal loss [52], or applied to a "blobbed" version of the desired boolean volume e.g. by placing a disk  
 132 around each GT position [53–55]. Alternative methods take a soft version of the binary classification

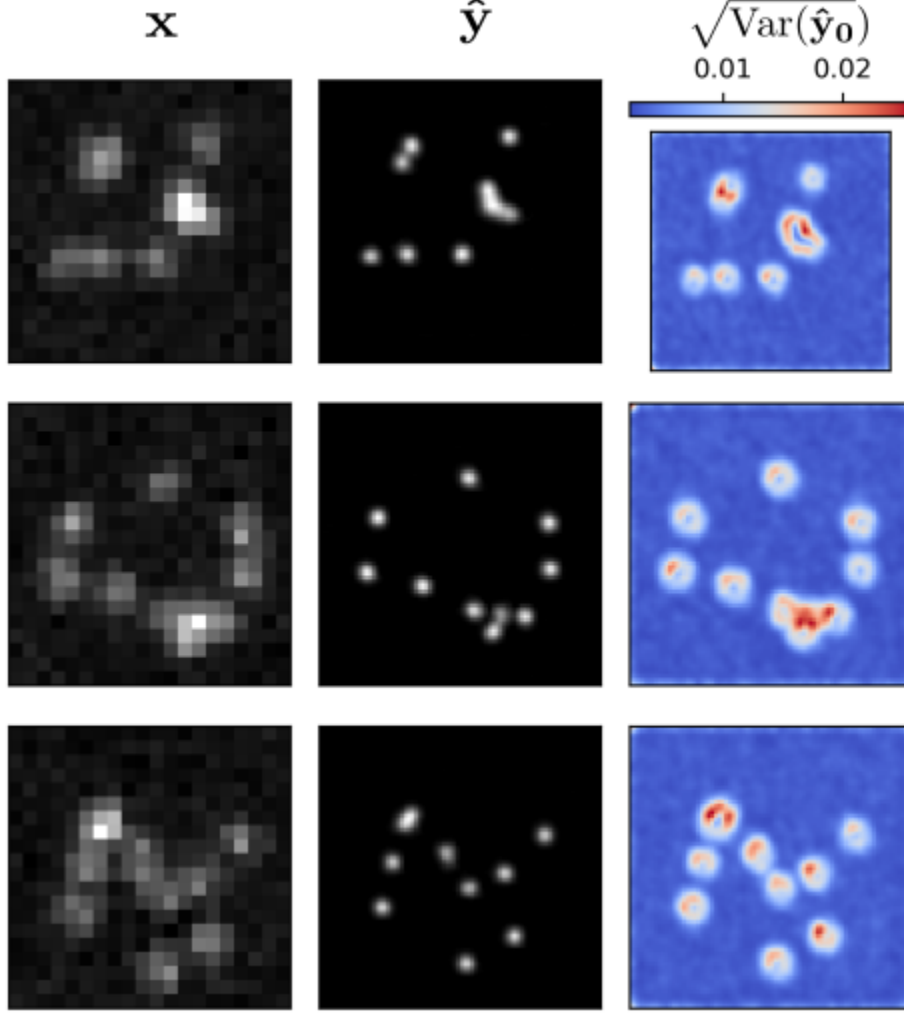


Figure 3: Kernel density estimates for various signal to noise ratios (SNR)

problem. That is, by placing a small Gaussian around each GT position (e.g. with std of 1 pixel), and matching continuous heatmaps, backpropagation yields more meaningful gradients and eases the learning process convergence.

Localization heatmaps thus form a natural encoding for SMLM images, which can be input to our conditional diffusion model. Therefore, to encode raw data  $\mathbf{x}$  into a more tractable representation, we train the DeepSTORM architecture (Nehme 2020). Raw coordinates  $\theta$  are binned into an upsampled image  $\mathbf{z}$ .

$$\mathcal{L}(\mathbf{y}, \hat{\mathbf{y}}) = \|\mathbf{y} - \hat{\mathbf{y}}\|^2$$

## 5 Experiments

Training data was simulated under the image degradation model, drawing coordinates uniformly over a disc. We set  $T = 100$  for all experiments and treat forward process variances  $\beta_t$  as hyperparameters, with a linear schedule from  $\beta_0 = 10^{-4}$  to  $\beta_T = 10^{-2}$ . These constants were chosen to be small relative to data scaled to  $[-1, 1]$ , ensuring that reverse and forward processes have approximately the same functional form while keeping the signal-to-noise ratio at  $x_T$  as small as possible ( $L_T = D_{KL}(q(x_T|x_0)||\mathcal{N}(0, I)) \approx 10^{-5}$  bits per dimension in our experiments).

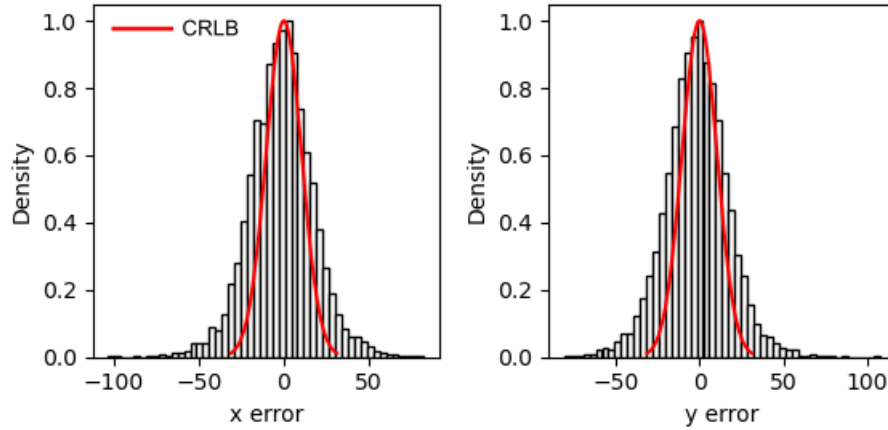


Figure 4: Localization errors of the trained model

To represent the reverse process, we used the DDPM architecture based on a U-Net backbone (Ho 2020). Parameters are shared across time, which is specified to the network using the Transformer sinusoidal position embedding  $\gamma$ . We use self-attention at the  $16 \times 16$  feature map resolution  $\gamma$ . Details are in Appendix A.

and the channel multipliers at different resolutions (see Appendix A for details). To condition the model on the input  $x$ , we up-sample the low-resolution image to the target resolution using bicubic interpolation. The result is concatenated with  $y_t$  along the channel dimension. We experimented with more sophisticated methods of conditioning, such as using  $\gamma$ , but we found that the simple concatenation yielded similar generation quality.

## 6 Related Work

### 6.1 Diffusion Models

Prior work of diffusion models  $\gamma$  require 1-2k diffusion steps during inference, making generation slow for large target resolution tasks. We adapt techniques from  $\gamma$  to enable more efficient inference. Our model conditions on  $\gamma$  directly (vs  $t$  as in  $\gamma$ ), which allows us flexibility in choosing the number of diffusion steps, and the noise schedule during inference. This has been demonstrated to work well for speech synthesis  $\gamma$ , but has not been explored for images. For efficient inference, we set the maximum inference budget to 100 diffusion steps, and hyper-parameter search over the inference noise schedule. This search is inexpensive as we only need to train the model once  $\gamma$ . We use FID on held-out data to choose the best noise schedule, as we found PSNR did not correlate well with image quality.

## 7 Conclusion

## References

- [1] Nehme, E., et al. *DeepSTORM3D: dense 3D localization microscopy and PSF design by deep learning*. Nature Methods 17, 734–740 (2020).
- [2] Ouyang, W., et al. *Deep learning massively accelerates super-resolution localization microscopy*. Nature Biotechnology 36, 460–468 (2018).
- [3] Speiser, A., et al. *Deep learning enables fast and dense single-molecule localization with high accuracy*. Nature Methods 18, 1082–1090 (2021).
- [4] Sohl-Dickstein J., et al. *Deep unsupervised learning using nonequilibrium thermodynamics*. ICLR (2015).

176 [5] Ho J., et al. *Denoising Diffusion Probabilistic Models*. Advances in Neural Information Processing Systems  
177 (2015).

178 [6] Nanxin C., et al. *WaveGrad: Estimating Gradients for Waveform Generation*. ICLR (2021).

179 [4] Chao, J., et al. *Fisher information theory for parameter estimation in single molecule microscopy: tutorial*.  
180 Journal of the Optical Society of America A 33, B36 (2016).

181 [5] Schermelleh, L. et al. *Super-resolution microscopy demystified*. Nature Cell Biology vol. 21 72–84 (2019).

182 [6] Zhang, B., et al. *Gaussian approximations of fluorescence microscope point-spread function models*. (2007).

183 [7] Smith, C.S., *Fast, single-molecule localization that achieves theoretically minimum uncertainty*. Nature  
184 Methods 7, 373–375 (2010).

185 [8] Nieuwenhuizen, R., et al. *Measuring image resolution in optical nanoscopy*. Nature Methods 10, 557–562  
186 (2013).

187 [9] Huang, F., et al. *Video-rate nanoscopy using sCMOS camera-specific single-molecule localization algorithms*.  
188 Nat Methods 10, 653–658 (2013).

189 [10] Rust, M., et al. *Sub-diffraction-limit imaging by stochastic optical reconstruction microscopy (STORM)*.  
190 Nat Methods 3, 793–796 (2006).

191 [11] Betzig, E., et al. *Imaging intracellular fluorescent proteins at nanometer resolution*. Science 313, 1642–1645  
192 (2006).

193 [12] Weigert, M., et al. *Content-aware image restoration: pushing the limits of fluorescence microscopy*. Nat.  
194 Methods 15, 1090 (2018).

195 [13] Falk, T., et al. *U-net: deep learning for cell counting, detection, and morphometry*. Nat. Methods 16, 67–70  
196 (2019).

197 [14] Boyd, N., et al. *DeepLoco: fast 3D localization microscopy using neural networks*. Preprint at bioRxiv  
198 <https://doi.org/10.1101/267096> (2018)

199 [15] Zelger, P., et al. *Three-dimensional localization microscopy using deep learning*. Opt. Express 26,  
200 33166–33179 (2018)

201 [16] Zhang, P., et al. *Analyzing complex single-molecule emission patterns with deep learning*. Nat. methods 15,  
202 913 (2018)

203 [17] Saharia, C., et al. *Image Super-Resolution via Iterative Refinement*. Preprint at arXiv  
204 <https://doi.org/10.48550/arXiv.2104.07636> (2021)

## 205 A Appendix

206 Standard SMLM localization algorithms based on maximum likelihood estimators or least squares  
207 optimization require tight control of activation and reactivation to maintain sparse emitters, presenting  
208 a tradeoff between imaging speed and labeling density. Recently, deep models have generalized  
209 SMLM to densely labeled structures by predicting high-resolution kernel density estimates (KDEs)  
210 from low resolution images with convolutional networks. However, estimated KDEs may contain  
211 irregularities due to finite sample sizes and limited model capacity. Denoising diffusion probabilistic  
212 models (DDPMs) are well suited conditional super resolution tasks, demonstrating promising results  
213 in detail reconstruction, while directly providing uncertainties in model predictions.

214 Single molecule localization microscopy (SMLM) relies on the temporal resolution of fluorophores  
215 whose spatially overlapping point spread functions would otherwise render them unresolvable  
216 at the detector. Common strategies for the temporal separation of molecules involve molecular  
217 photoswitching from dark to fluorescent states, permitting resolution of fluorophores beyond the  
218 diffraction limit. Estimation of molecular coordinates is typically carried out by modeling the optical  
219 impulse response of the imaging system and fitting model functions to the data. However, such  
220 models are only well-suited to isolated molecules, reducing the number of molecules in the field of  
221 view and limiting temporal resolution in super resolution microscopy. This issue has incited a series  
222 of efforts to increase the density of fluorescent molecules imaged in a single frame while developing  
223 appropriate models for dense localization.

224 In fluorescence microscopy, each pixel is treated as a Poisson random variable (Smith 2010; Nehme  
225 2020; Chao 2016), with expected value

$$\omega = i_0 \int O(u)du \int O(v)dv \quad (10)$$

where  $i_0 = \eta N_0 \Delta$ . The scalar parameters  $\eta, \Delta$  are the photon detection probability of the sensor and the exposure time, respectively. Without loss of generality, we assume  $\eta = \Delta = 1$ . Most importantly,  $N_0$  represents the signal amplitude, which we assume maintains a fixed value. The optical impulse response  $O(u, v)$  is often approximated as a 2D isotropic Gaussian with standard deviation  $\sigma$  (Zhang 2007). This approximation has the convenient property, that the effects of pixelation can be expressed in terms of error functions. For example, given a fluorescent emitter located at  $\theta = (u_0, v_0)$ , we have that

$$\int O(u)du = \frac{1}{2} \left( \operatorname{erf} \left( \frac{u_k + \frac{1}{2} - u_0}{\sqrt{2}\sigma} \right) - \operatorname{erf} \left( \frac{u_k - \frac{1}{2} - u_0}{\sqrt{2}\sigma} \right) \right) \quad (11)$$

where we have used the common definition  $\operatorname{erf}(z) = \frac{2}{\sqrt{\pi}} \int_0^z e^{-t^2} dt$ . Our generative model also incorporates a normally distributed white noise per pixel  $\zeta$  with offset  $o$  and variance  $\sigma^2$ . Ultimately, we have a Poisson component of the signal, which scales with  $N_0$  and a Gaussian component, which does not.

Consider,

$$\zeta_k - o_k + \sigma_k^2 \sim \mathcal{N}(\sigma_k^2, \sigma_k^2) \approx \text{Poisson}(\sigma_k^2) \quad (12)$$

Since  $\mathbf{x}_k = \mathbf{s}_k + \zeta_k$ , we transform  $\mathbf{x}'_k = \mathbf{x}_k - o_k + \sigma_k^2$ , which is distributed according to